
Figures and figure supplements

SWI/SNF senses carbon starvation with a pH-sensitive low-complexity sequence

J Ignacio Gutierrez et al

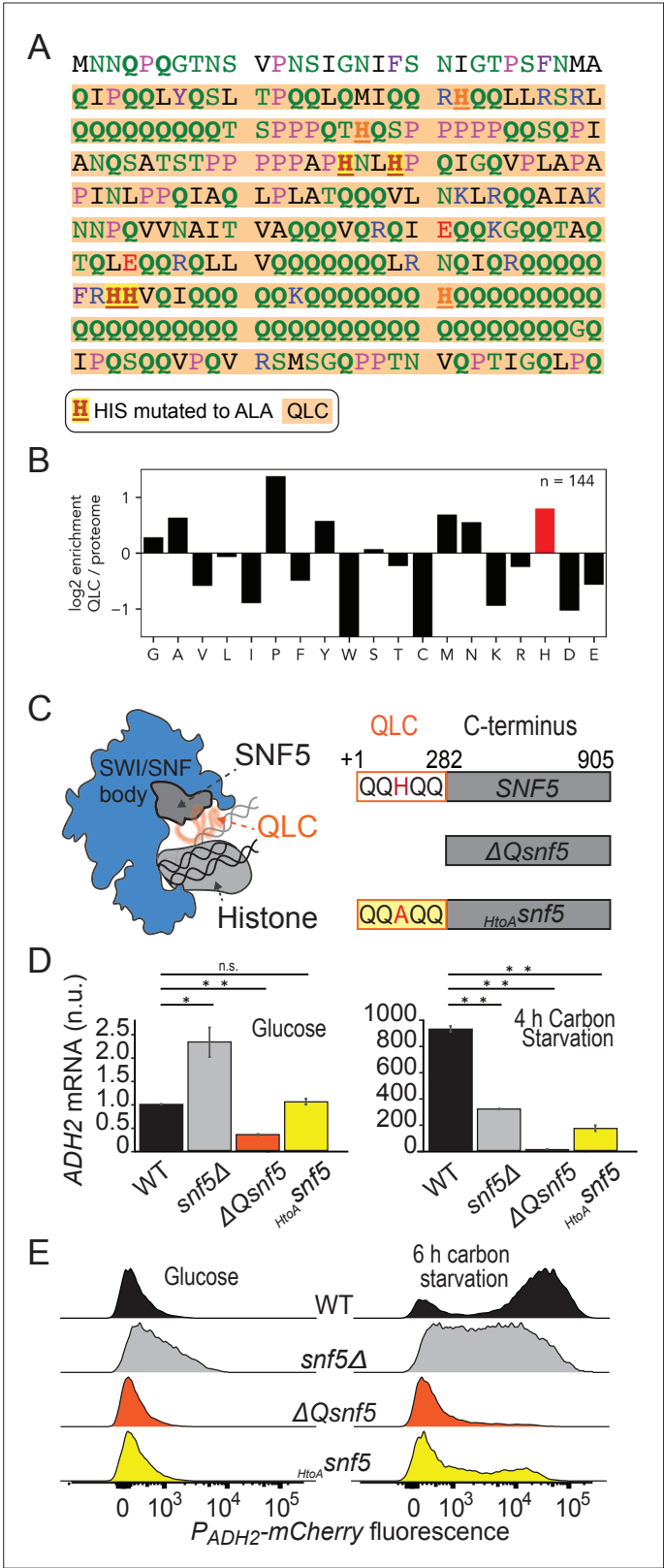


Figure 1. Efficient induction of ADH2 upon glucose starvation requires the SNF5 glutamine-rich low-complexity sequence with native histidines. **(A)** Sequence of the N-terminal low-complexity domain of SNF5. This domain was deleted in the ΔQsnf5 strain. The glutamine-rich domain is highlighted in orange. The 4/7 histidines that were mutated to alanine in the HtoASNF5 allele are highlighted in red. **(B)** The log₂ of the frequency of each amino

Figure 1 continued on next page

Figure 1 continued

acid within QLCs divided by the global frequency of each amino acid in the proteome (*S. cerevisiae*). Values > 0 indicate enrichment in QLCs. **(C)** Left: schematic of the SWI/SNF complex engaged with a nucleosome. The *SNF5* C-terminus is shown in gray, while the disordered N-terminal QLC is shown in orange. Right: schematic of the three main *SNF5* alleles used in this study. **(D)** RT-qPCR results assessing levels of endogenous *ADH2* mRNA in four strains grown in glucose (left) or after 4 hr of glucose starvation (right). Note: y-axes are different for each plot. **(E)** Representative histograms (10,000 cells) showing the fluorescent signal from a *P_{ADH2}-mCherry* reporter gene for four strains grown in glucose (left) or after 6 hr of glucose starvation (right). Statistical tests are Bonferroni-corrected *t*-tests, **p*<0.05, ***p*<0.01, n.s., not significant.

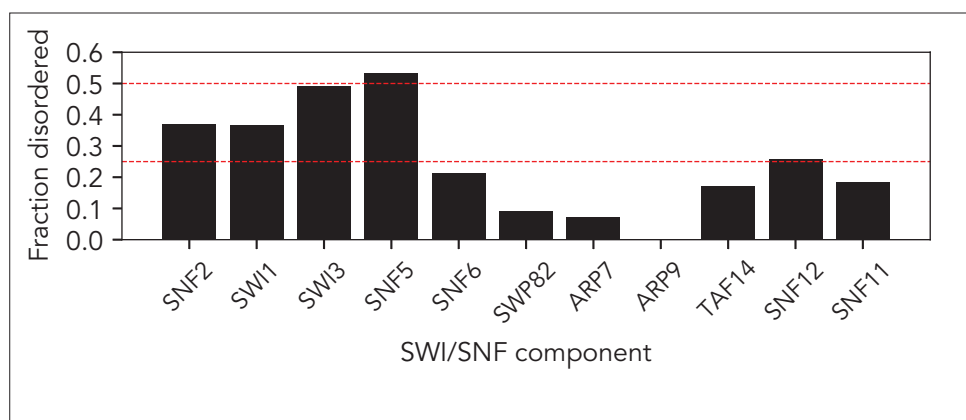


Figure 1—figure supplement 1. The SWI/SNF complex has 10/11 subunits with significant disorder. Fractional disorder in each of the core 11 SWI/SNF components. Dashed red lines represent 25% and 50% disorder. 5 of the 11 components contain over 25% disorders. Disorder prediction performed using metapredict (see Materials and methods).

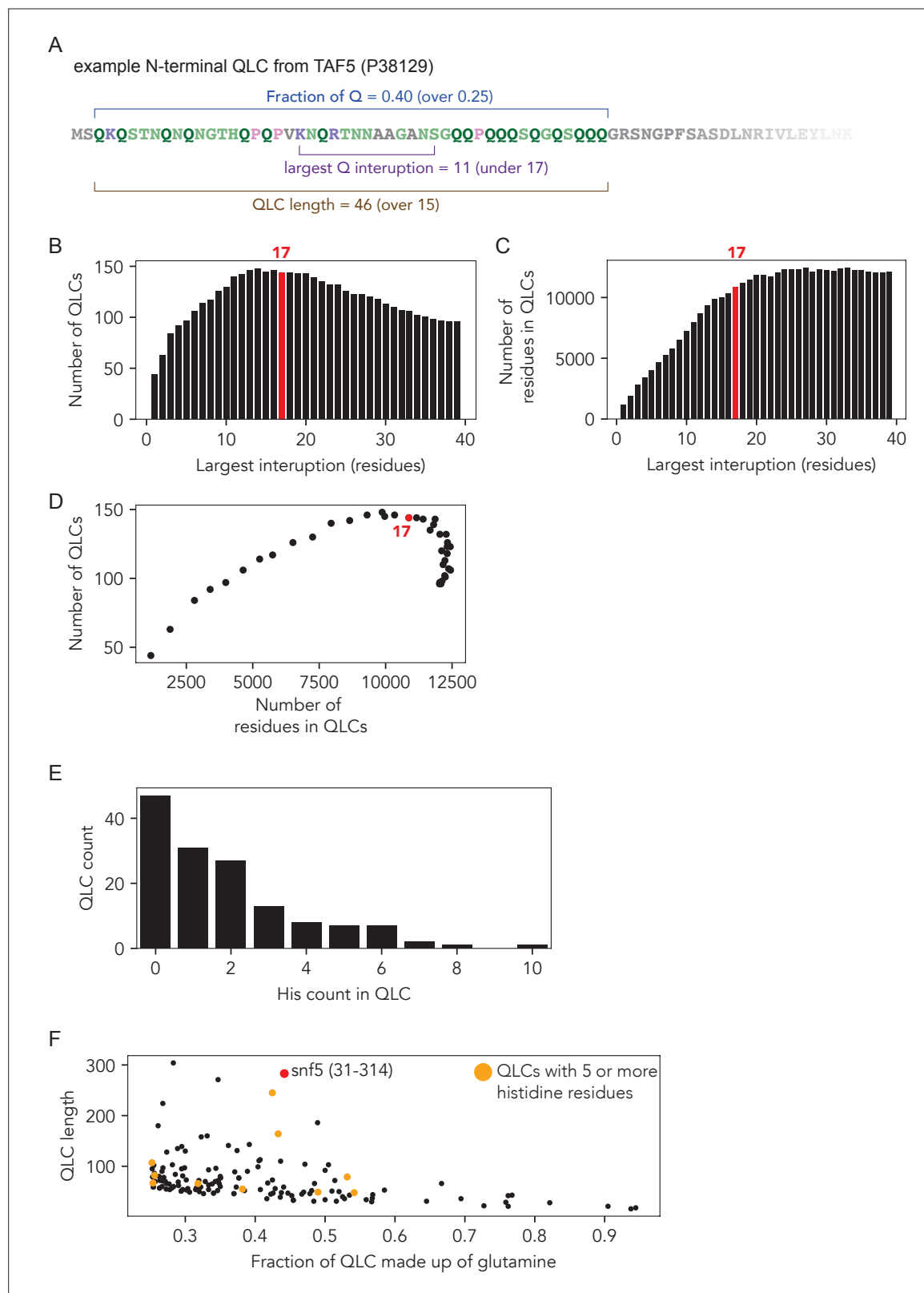


Figure 1—figure supplement 2. Identification and analysis of glutamine-rich low-complexity sequences (QLCs). **(A)** Example of a QLC region with the criteria that define QLCs annotated: QLCs were defined as subregions of the proteome in which they have an average fraction of glutamine residues of 25% or higher (minimum fraction, e.g., here 40%), the maximum interruption between any two glutamine residues is less than 17 residues (e.g., here 11 residues), and the whole QLC is at least 15 residues in length (minimum length, e.g., here 46). **(B–D)** Computational analysis used to select

Figure 1—figure supplement 2 continued on next page

Figure 1—figure supplement 2 continued

the interruption length criterion for QLC identification. Systematic variation revealed that a maximum interruption disruption length of 17 residues optimized the number of QLCs identified (**B**) and the number of residues found within QLCs (**C**), offering an optimally permissive value under the 0.25 or greater fraction of glutamine threshold. (**D**) Number of residues in QLCs vs. number of QLCs shows that an interruption length of 17 sits at an optimum for both parameters. (**E**) Histogram of the number of histidine residues within *S. cerevisiae* QLCs (n = 144). (**F**) Most QLCs contain relatively few histidine, but a small fraction contain five or more.

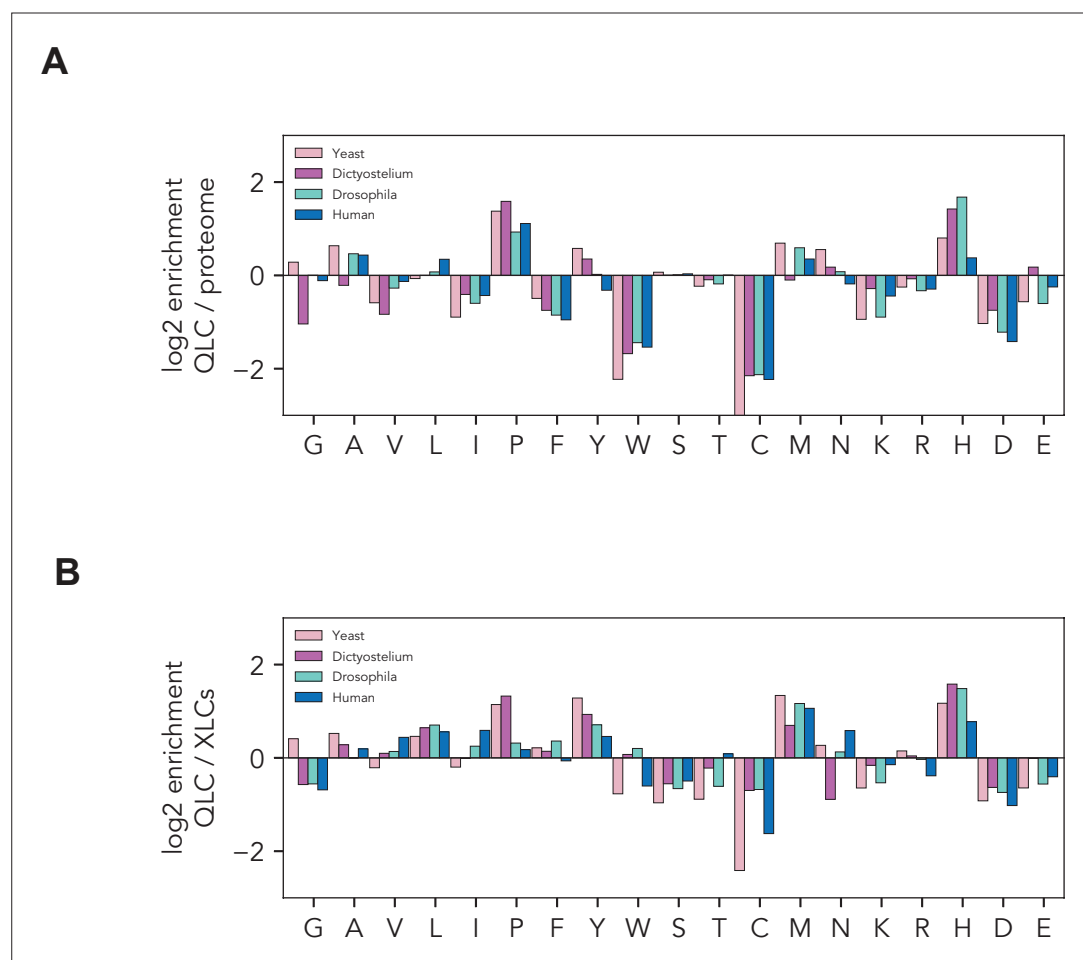


Figure 1—figure supplement 3. Histidines are enriched in glutamine-rich low-complexity sequences. Amino acid frequencies within glutamine-rich low-complexity sequences (QLCs) in *S. cerevisiae* (yeast), *Dictyostelium discoideus*, *Drosophila melanogaster*, and humans. **(A)** Enrichment of each amino acid in QLCs compared to global amino acid frequencies in each proteome. **(B)** Enrichment of each amino acid in QLCs compared to amino acid frequencies in all low-complexity sequences identified using Wootton–Federhen complexity (see Materials and methods).

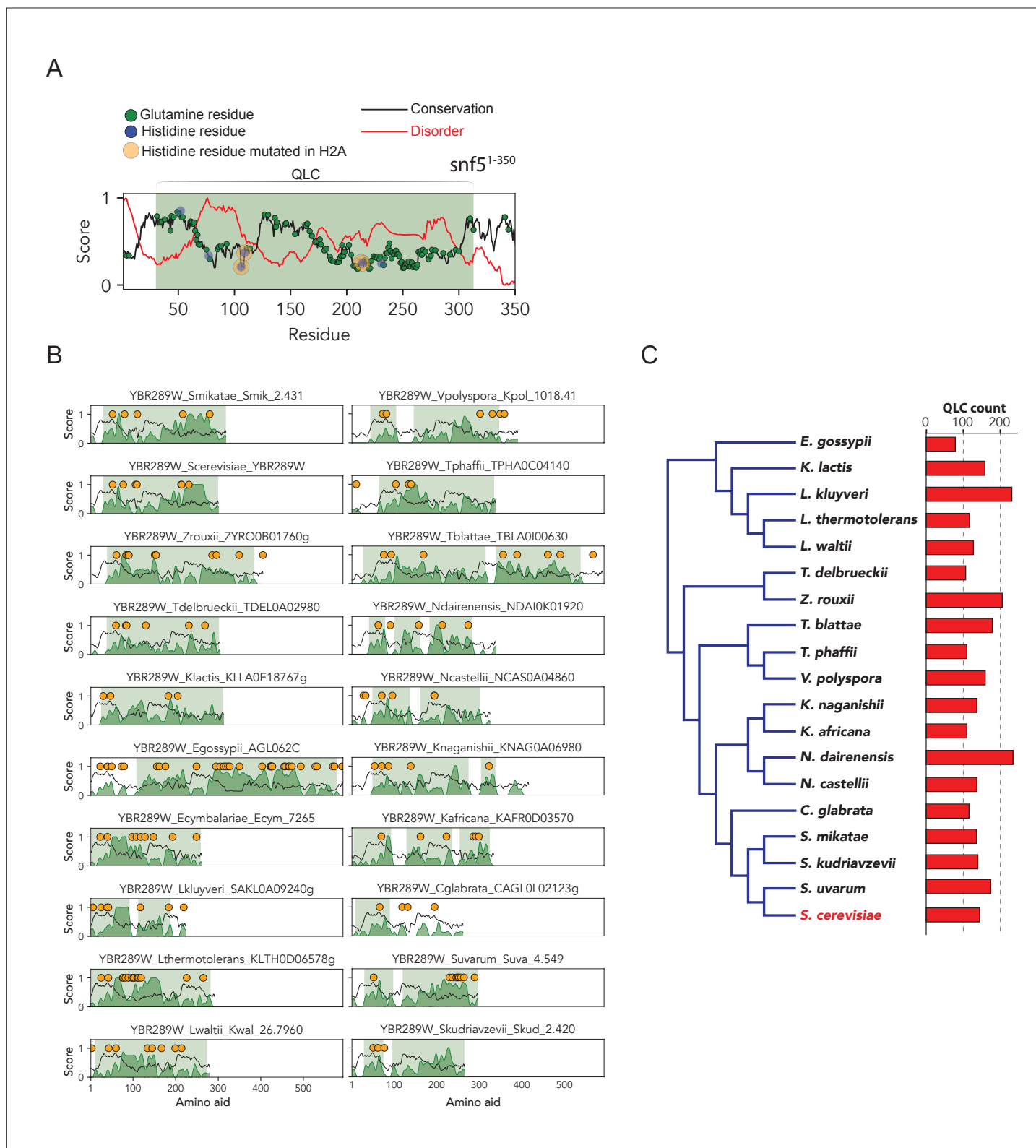


Figure 1—figure supplement 4. The SNF5 N-terminal glutamine-rich low-complexity domain (with embedded histidines) is broadly conserved across Ascomycota. **(A)** Analysis of SNF5 N-terminal region showing conservation (black), disorder (red), glutamine positions (green), histidine positions (blue), histidines that are mutated (orange), and the QLC (shaded green area). Four histidine residues are highlighted, which, when mutated to alanine, lead to a phenotypic change. Intriguingly, these four histidines are located in highly disordered and poorly conserved subregions of the SNF5 N-terminal region. **(B)** The same analysis for 19 ascomycetes. **(C)** Phylogeny of ascomycetes analyzed above, with the total number of QLCs identified in each proteome shown to the right.

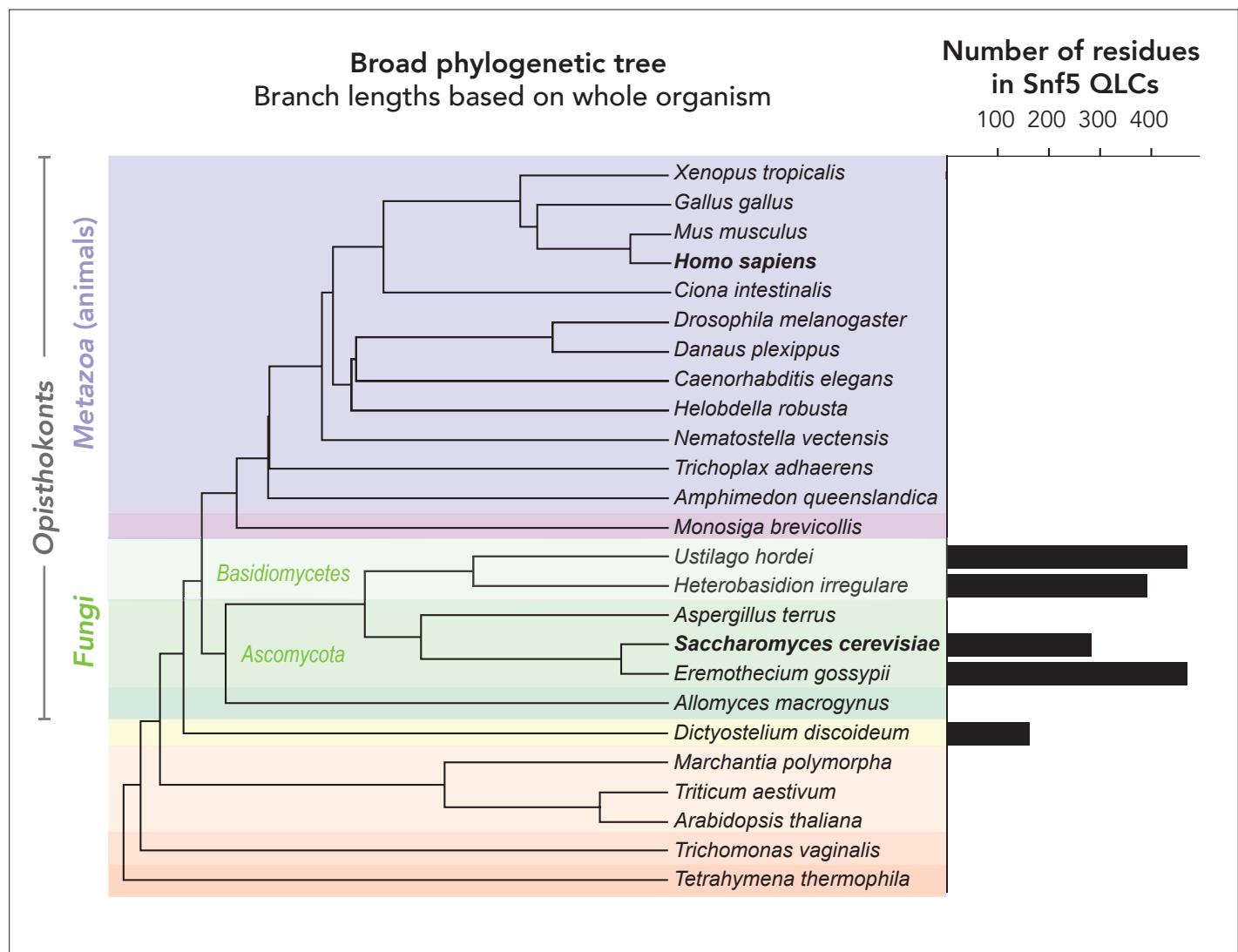


Figure 1—figure supplement 5. The SNF5 N-terminal glutamine-rich low-complexity domain was probably gained in the fungal lineage. Broad orthologs of SNF5 were determined using the more conserved C-terminal domain. These orthologs were analyzed, and if QLCs were detected, the number of residues within is plotted in the bar graph to the right. The Ascomycota and Basidiomycota both have QLCs, possibly indicating gain of the domain in this lineage. There is no evidence of SNF5 QLCs in the Metazoa (animals) or in the closest outgroup to the Metazoa (Choanoflagellates, i.e., *Monosiga brevicollis*). The slime mold amoeba *Dictyostelium discoideum* has an SNF5 QLC, but this organism is extremely rich in glutamine repeats, and it is not clear that this QLC has the same origin as the fungal clade.

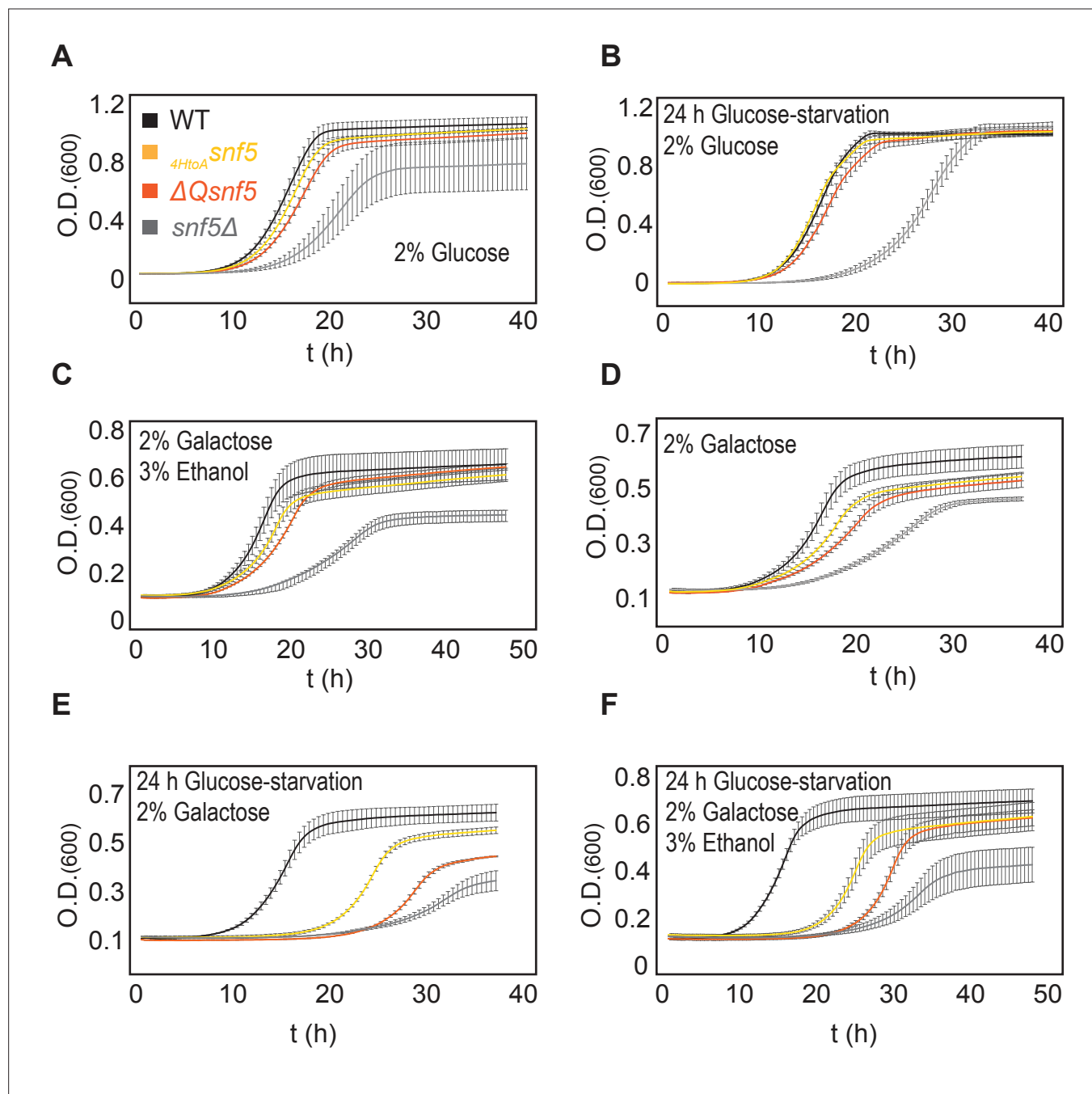


Figure 1—figure supplement 6. The *SNF5* QLC is important for recovery from carbon starvation. Growth rate was assessed in a plate reader in various conditions. (A) Comparison of growth rate of WT, $\Delta Qsnf5$, $4HtoA snf5$, and $snf5\Delta$ strains in synthetic complete media with glucose. (B) Cells were grown to log phase, carbon-starved for 24 hr, and then grown in 2% glucose. (C, D) Cells were immediately switched from glucose to poor carbon sources. (E, F) Cells were subjected to acute starvation for 24 hr and then switched to poor carbon sources.

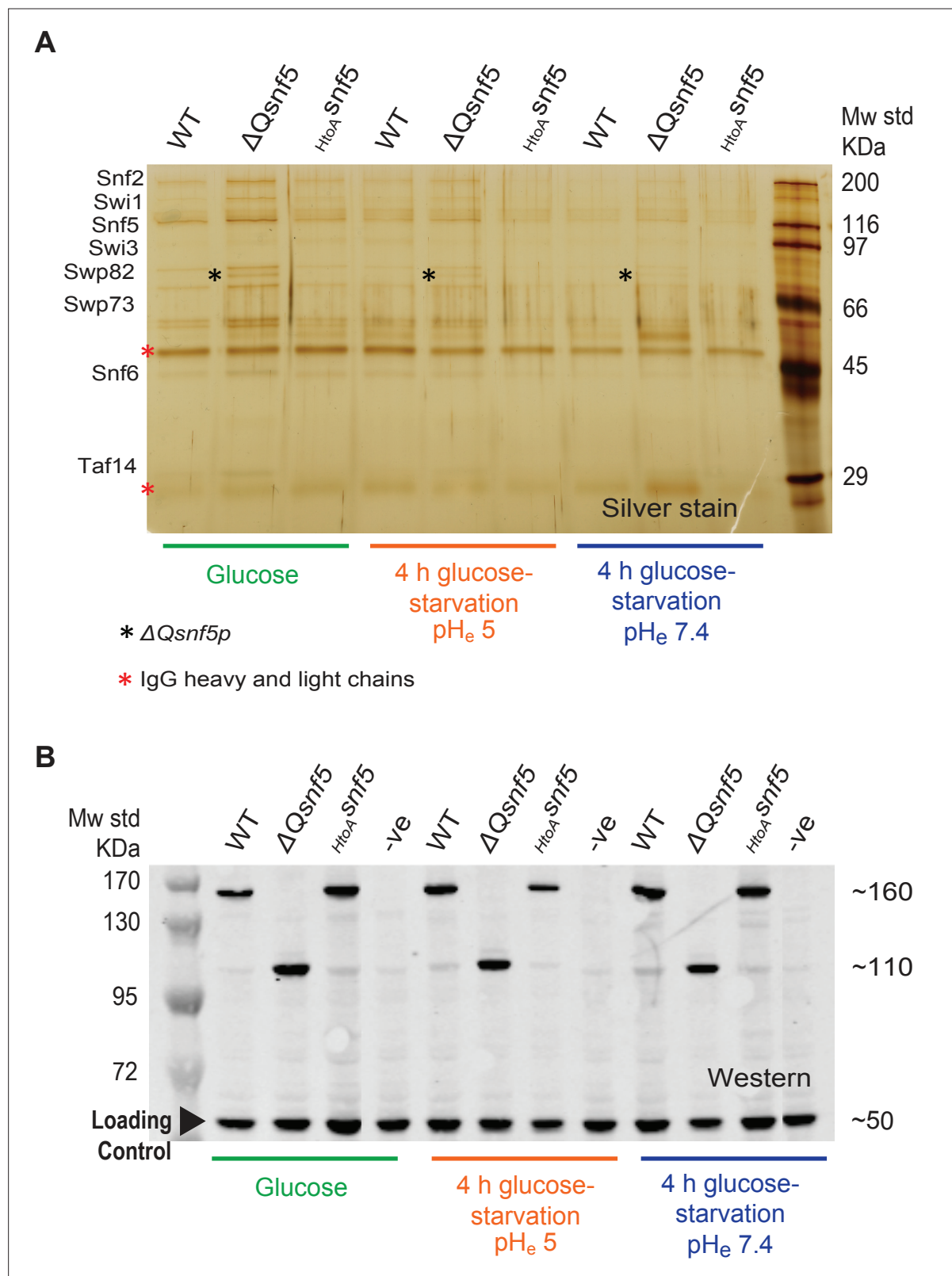


Figure 1—figure supplement 7. Mutation of the *SNF5* QLC does not lead to protein degradation or loss of SWI/SNF complex integrity. **(A)** The entire SWI/SNF complex copurifies with *SNF2* in all strains and conditions. The endogenous *SNF2* gene was tandem affinity purification (TAP)-tagged at the C-terminus and used to immunoprecipitate the SWI/SNF complex from WT, Δ Qsnf5, or *HtoA snf5* strains either exponentially growing in glucose or after 4 hr acute carbon starvation in media titrated to pH_e 5 or 7.4 (indicated at bottom). A silver stain of an SDS-PAGE analysis is shown. **(B)** Neither *SNF5* nor

Figure 1—figure supplement 7 continued on next page

Figure 1—figure supplement 7 continued

its mutant alleles are degraded upon glucose starvation. Western blots of the TAP-tagged *SNF5* alleles in various conditions (indicated at bottom). TAP-tagged ΔQ -*snf5* runs at ~110 kDa, 288 amino acids smaller than WT (~160 kDa). An anti-glucokinase antibody was used as a loading control (bottom band at ~50 kDa).

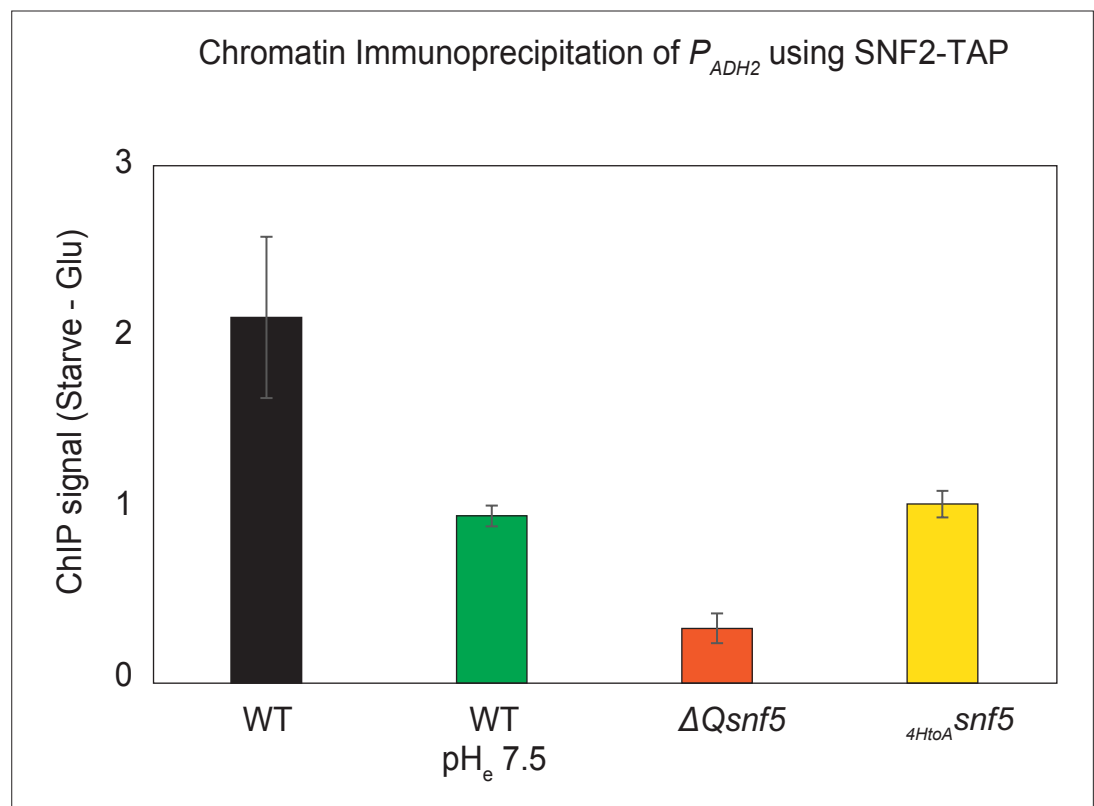


Figure 1—figure supplement 8. Efficient recruitment of the SWI/SNF complex to the *ADH2* promoter depends upon pH, the *SNF5* QLC and histidines within. The endogenous *SNF2* gene was tandem affinity purification (TAP)-tagged at the C-terminus and used to immunoprecipitate the SWI/SNF complex from WT, $\Delta Qsnf5$, or $^{4HtoA}snf5$ strains. Prior to immunoprecipitation, chromatin and proteins were crosslinked with formaldehyde, enabling co-purification of chromatin associated with the SWI/SNF complex (chromatin immunoprecipitation [ChIP]). Quantitative polymerase chain reaction (qPCR) was then performed with primers specific to the *ADH2* promoter. The y-axis shows the difference in qPCR signal in strains grown in glucose minus the signal after 4 hr of acute carbon starvation. Values greater than 1 indicate recruitment of SWI/SNF to the *ADH2* promoter upon carbon starvation. Experiments were performed in media titrated to pH_e 5 or 7.4 (indicated on the x-axis). n = 3, standard deviation is shown.

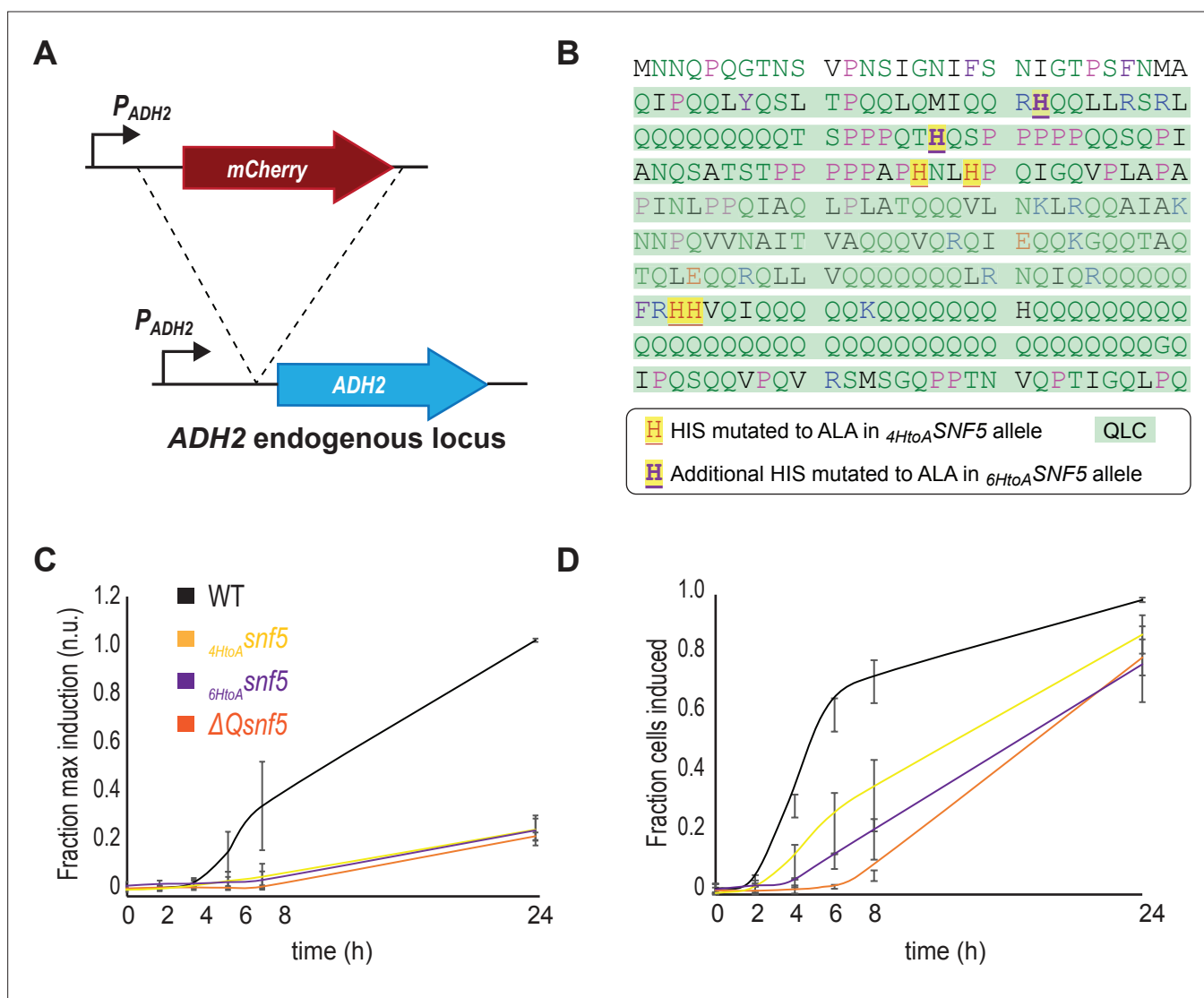


Figure 1—figure supplement 9. The *SNF5* QLC and embedded histidines are required for efficient *ADH2* induction upon carbon starvation. **(A)** Schematic of the P_{ADH2} -*mCherry* reporter gene: the reporter construct was integrated into the endogenous *ADH2* locus, resulting in a tandem repeat of the reporter gene followed by an intact *ADH2* gene. **(B)** Sequence of the *SNF5* N-terminus with the 4/7 histidines that were mutated in the *4HtoA* *snf5* allele highlighted as red on yellow, and the additional two histidines that were mutated in the *6HtoA* *snf5* allele highlighted as purple on yellow. **(C)** P_{ADH2} -*mCherry* induction during carbon starvation assessed by fluorescence cytometry, normalized to the maximal induction (median *mCherry* fluorescence at 24 hr in *SNF5* WT strains). **(D)** The fraction of the cells that induce P_{ADH2} -*mCherry* induction at each time point during carbon starvation (see Materials and methods). The *SNF5* alleles compared are WT, $\Delta Qsnf5$, *4HtoA* *snf5* (referred to in the rest of the article as simply *HtoA* *snf5*), and the *6HtoA* *snf5* strains with an additional two histidines (6/7 total) mutated to alanine. There is no significant difference between the *4HtoA* *snf5* and *6HtoA* *snf5* strains in these experiments. Mean and standard deviation are shown in each plot.

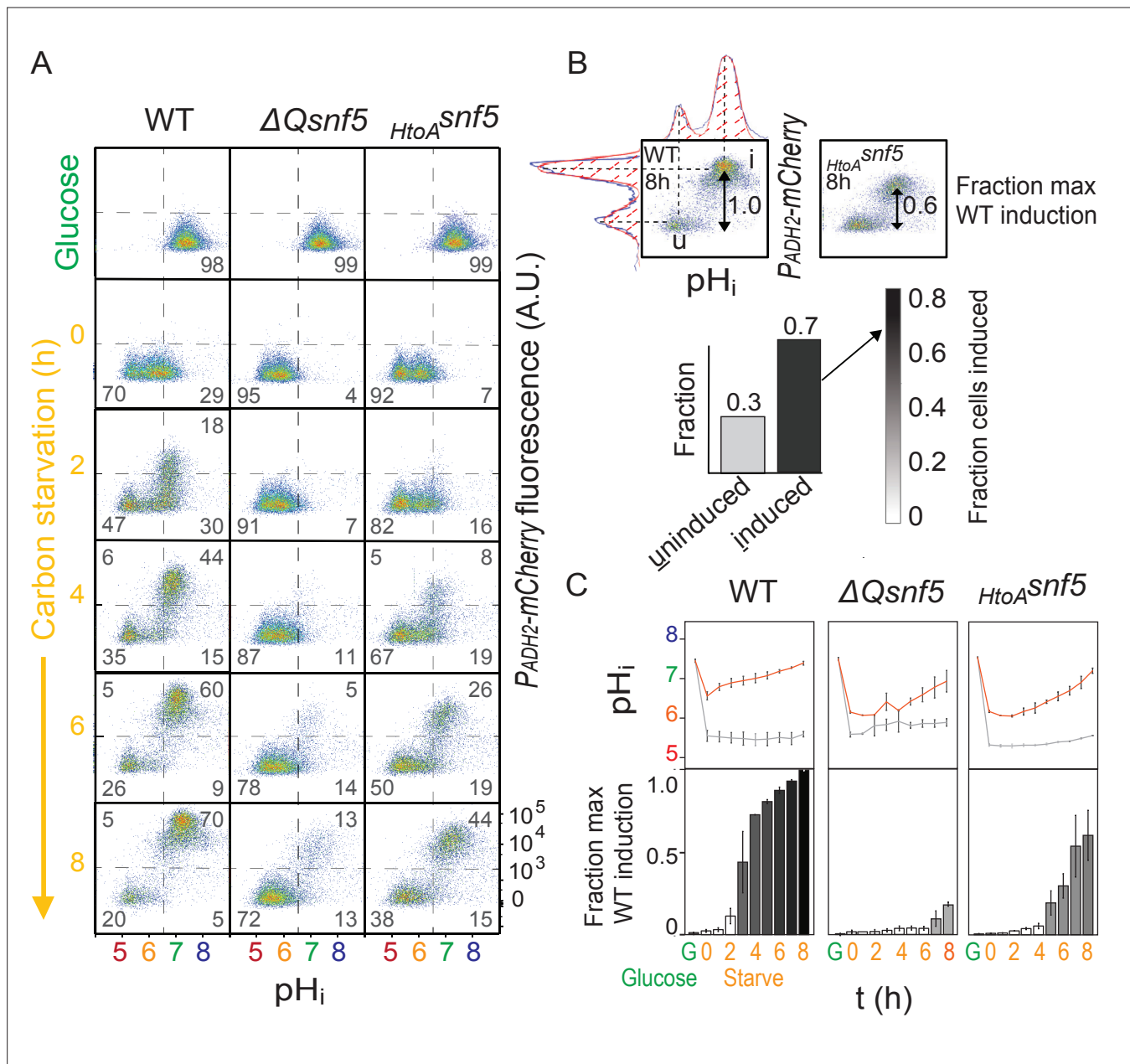


Figure 2. The SNF5 QLC is required for ADH2 expression and recovery of neutral pH. **(A)** Representative flow cytometry for WT, $\Delta Qsnf5$, or $HtoA^{snf5}$ strains: the x-axis shows nucleocytoplasmic pH (pH_i), while the y-axis shows fluorescence from the P_{ADH2} -mCherry reporter. Panels show cells grown in glucose (top) and then (second to bottom) after 0–8 hr of acute glucose starvation. Percentage of cells in each quadrant is indicated by gray numbers. **(B)** Schematic of quantification scheme: raw data from **(A)** was fit to a single or double Gaussian curve determined by a least-residuals method. **(C)** Quantification of pH_i and P_{ADH2} -mCherry expression during acute starvation. The median of each Gaussian for pH_i is plotted in **(C, top)**, black and gray lines are from induced and uninduced populations, respectively. The height of bars in **(C, bottom)** indicates the fraction of maximal P_{ADH2} -mCherry reporter gene expression (WT cells, 8 hr glucose starvation). The darkness of the bars indicates the fraction of the population in the induced versus uninduced state. Mean and standard deviation of three biological replicates are shown.

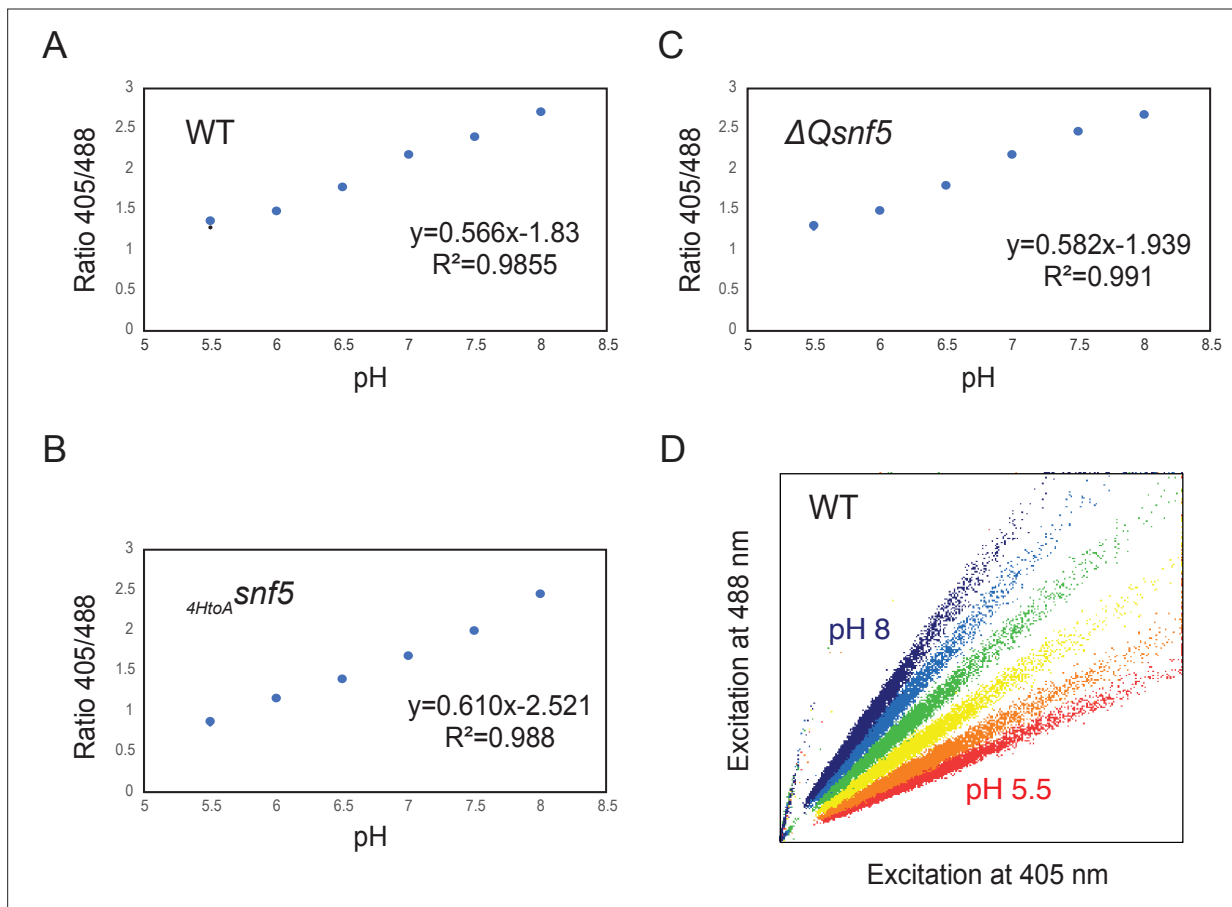


Figure 2—figure supplement 1. Examples of calibration curves to measure cytosolic pH using pHluorin. (A–C) Representative calibration curves to determine the ratio of fluorescence intensities at 405 and 488 nm in cells adjusted to a known pH by ATP depletion and permeabilization in buffers. The fluorescence properties of WT and mutant strains were slightly different; therefore, calibration curves were calculated for each strain: (A) WT, (B) $\Delta Qsnf5$, and (C) $4HtoA snf5$. (D) Shows representative scatterplots of fluorescence intensity obtained by cytometry from the WT strain.

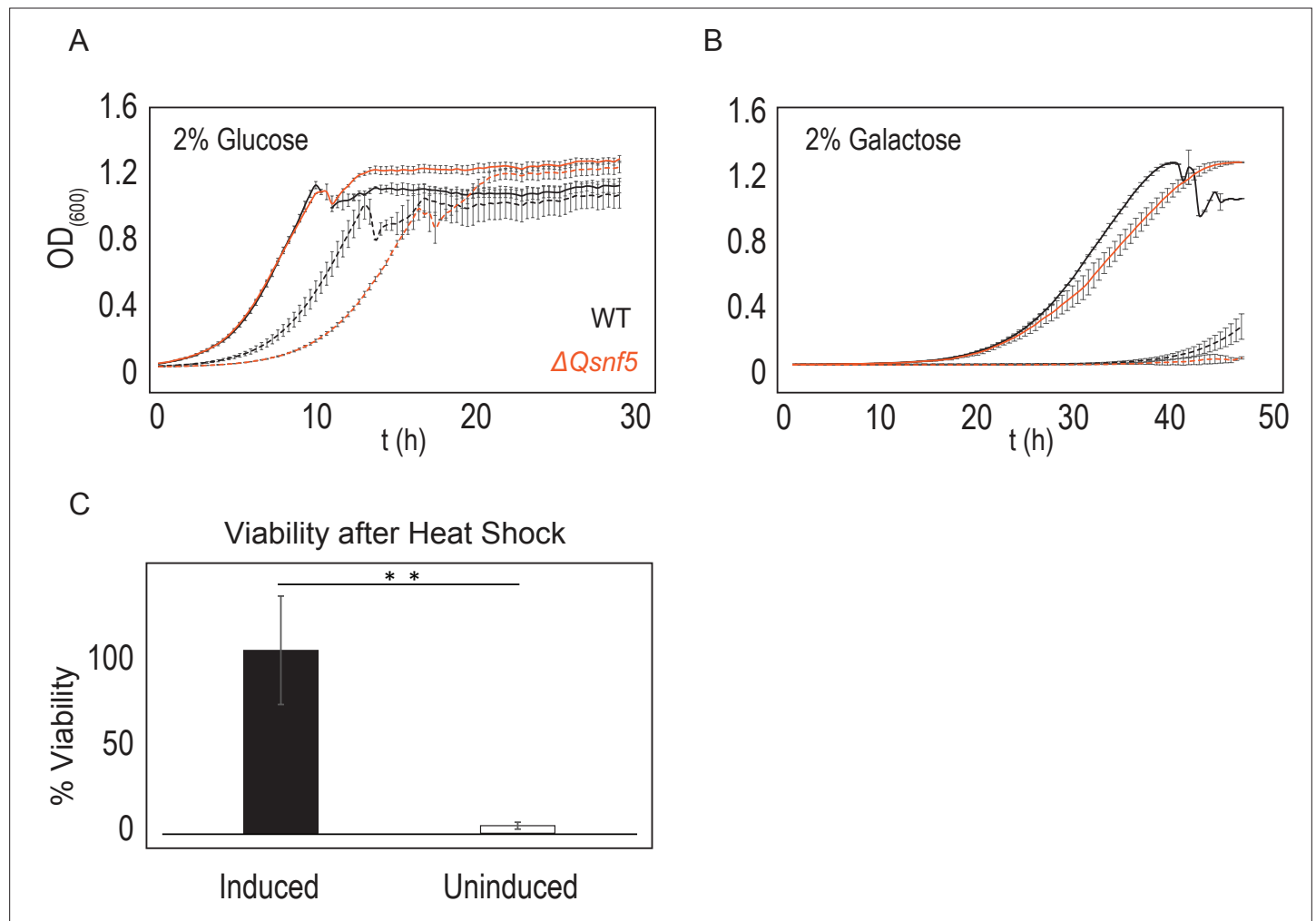


Figure 2—figure supplement 2. Cells that fail to induce P_{ADH2} -mCherry had lower fitness relative to the inducing population. 6 hr after acute carbon starvation, we used fluorescence-activated cell sorting (FACS) to separate equal numbers of cells with high (induced) and low (uninduced) mCherry fluorescence. **(A, B)** Uninduced cells (dashed lines) have lower growth rates than induced cells (solid lines). Black lines indicate WT strains, orange indicates $\Delta Qsnf5$ cells. **(A)** Comparison of growth rates in rich (2% glucose) media. **(B)** Comparison of growth rates in poor (2% galactose) media. **(C)** Uninduced cells have lower resistance to heat stress. Cells were subjected to heat shock for 15 min at 42°C followed by 3 min on ice, and then plated for single colonies. The number of colonies relative to unperturbed cells is plotted as % viability. Mean and standard deviation are shown, $n = 3$; statistical test is the Student's t -test, ** $p < 0.01$.

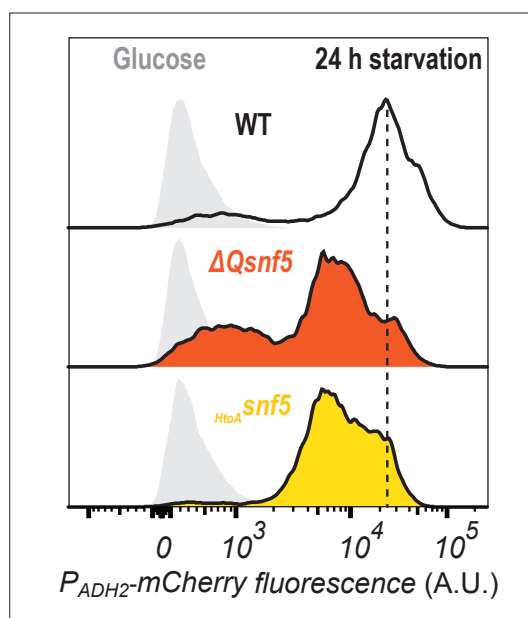


Figure 2—figure supplement 3. All strains ultimately express some amount of P_{ADH2} -mCherry reporter. Cytometry data showing P_{ADH2} -mCherry induction either in glucose (light gray peaks to left) or after 24 hr of carbon starvation (dark lines, and color coded by strain).

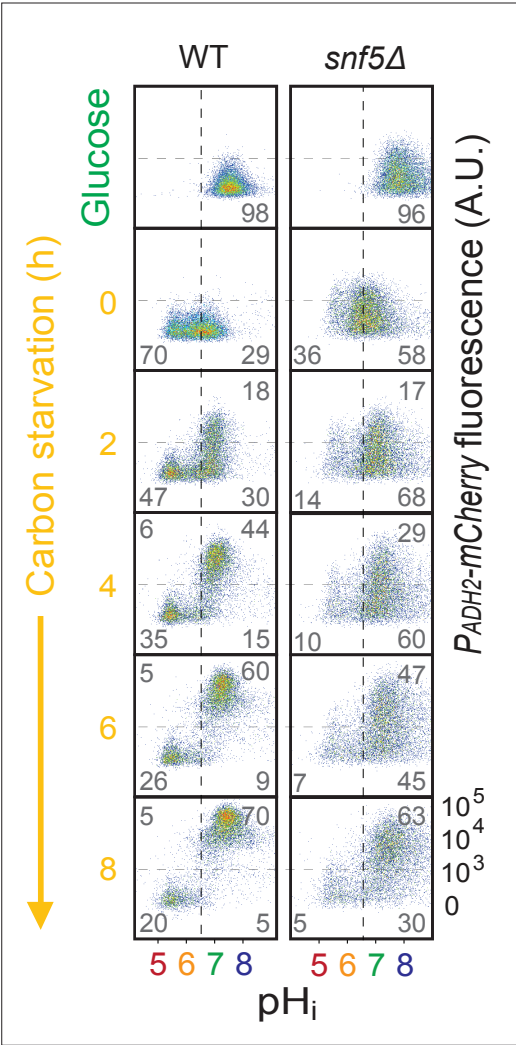


Figure 2—figure supplement 4. $snf5\Delta$ strains only had a slight delay in expression of the P_{ADH2} -mCherry reporter. Cytometry data showing P_{ADH2} -mCherry induction (y-axis) and nucleocytoplasmic pH (pH_i), calculated using the ratiometric pHluorin probe (x-axis), in WT (left) and $snf5\Delta$ (right) strains. Percentage of cells in each of the four quadrants is indicated.

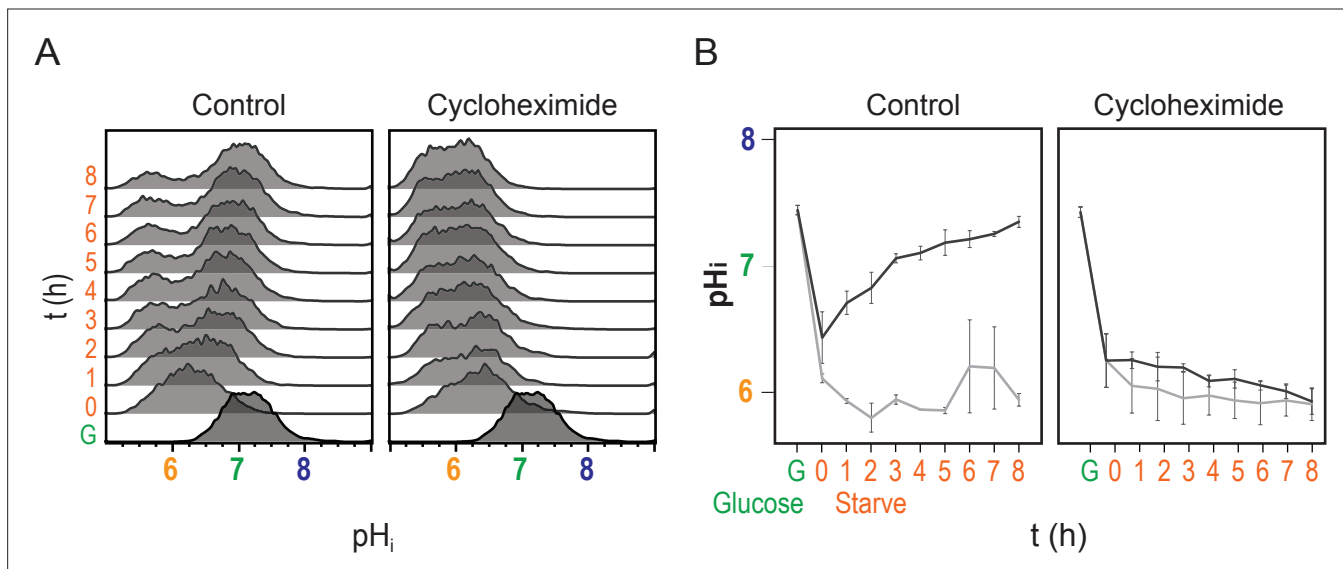


Figure 2—figure supplement 5. Recovery of pH_i requires new protein translation. **(A)** Cytometry data showing nucleocytoplasmic pH (pH_i), calculated using the ratiometric pHluorin probe. **(B)** Quantification of pH_i data (see Materials and methods), orange and gray lines are from induced and uninduced populations, respectively. Mean and standard deviation of three biological replicates are plotted. Cells were switched to acute carbon starvation media titrated to the optimal pH_e of 5.5 at time 0, but the right panels show cells additionally exposed to the translational inhibitor cycloheximide. Intracellular pH fails to recover without new protein translation.

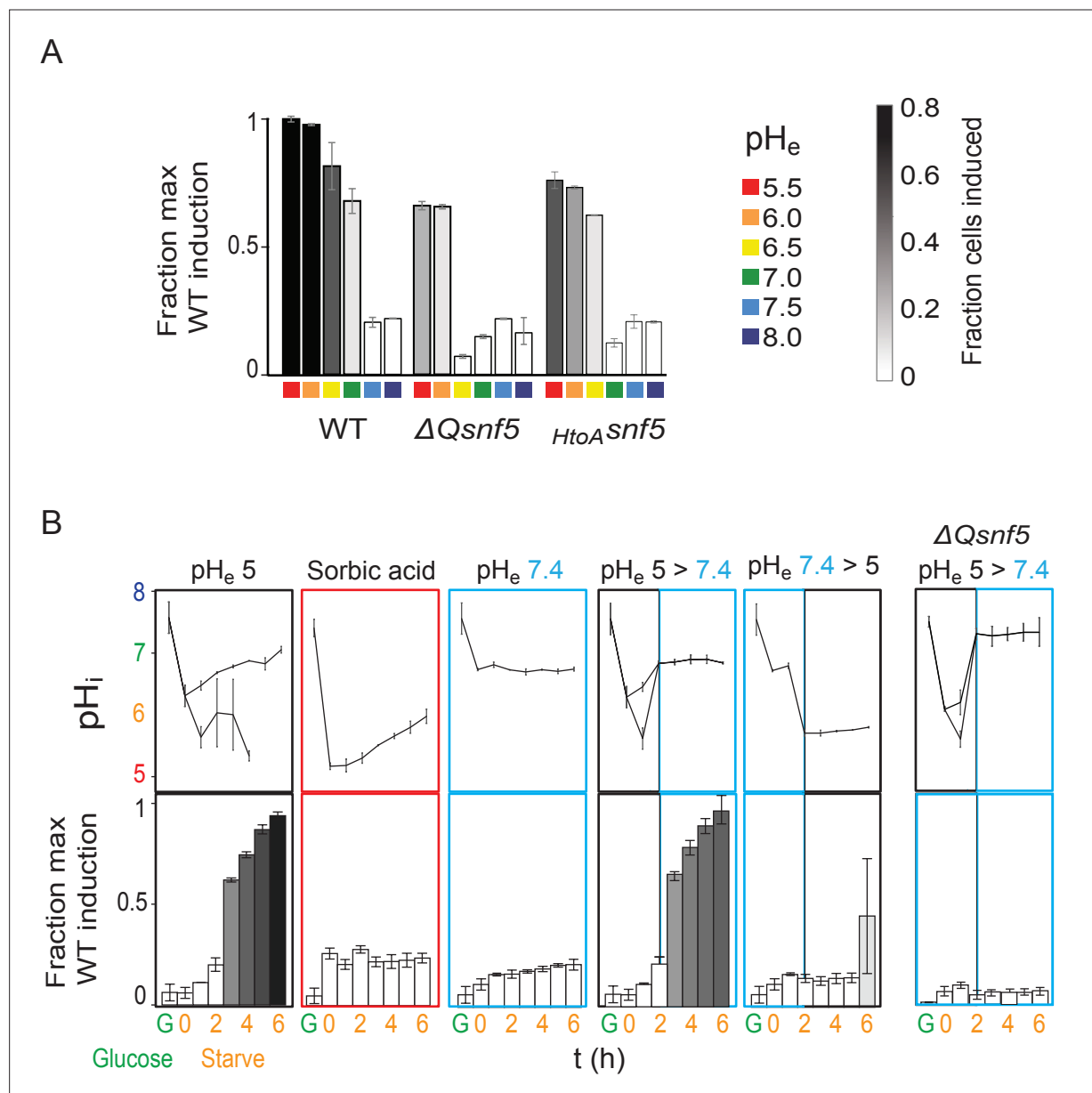


Figure 3. Transient acidification is required for *ADH2* induction upon carbon starvation. **(A)** Expression of *P_{ADH2}-mCherry* reporter gene in WT, $\Delta Qsnf5$, or $HtoA snf5$ strains 8 hr after acute carbon starvation in media titrated to various pH (pH_e , see legend, right). Bar height indicates the fraction of maximal *P_{ADH2}-mCherry* reporter gene expression (WT cells, pH_e 5.5). The darkness of the bars indicates the fraction of the population in the induced versus uninduced state (see legend, right). **(B)** Time courses of glucose starvation with media manipulations to perturb the intracellular pH response, either by changing media pH (pH_e) or by adding sorbic acid. Top panels show nucleocytoplasmic pH (pH_i), black and gray lines from induced and uninduced populations, respectively. Bottom panels quantify expression of the *P_{ADH2}-mCherry* reporter gene (as in **A**). All strains are WT except for the far-right panels, which are from a $\Delta Qsnf5$ strain.

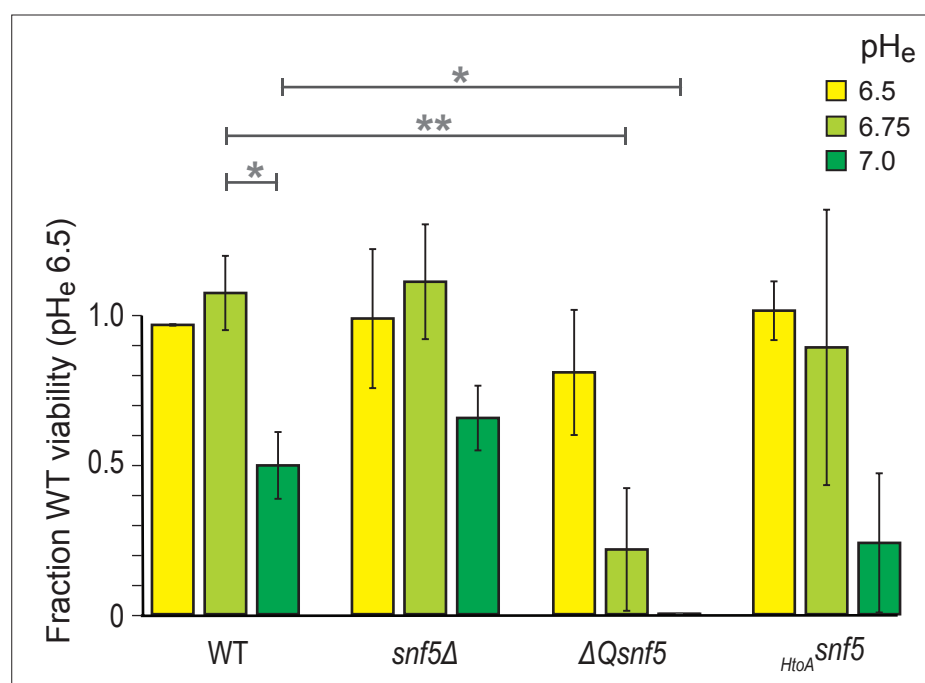


Figure 3—figure supplement 1. Deletion of the N-terminal glutamine-rich domain of *SNF5* renders cells hypersensitive to starvation at suboptimal extracellular pH. Cells were grown to log phase and then subjected to acute carbon starvation in media titrated to various pH_e values (see legend). After 24 hr starvation, cells were plated to determine the number of colony-forming units compared to WT cells starved at pH_e 6.5. Mean and standard deviation of three biological replicates are shown. * and ** represent p < 0.05 and p < 0.01, respectively, from t-tests.

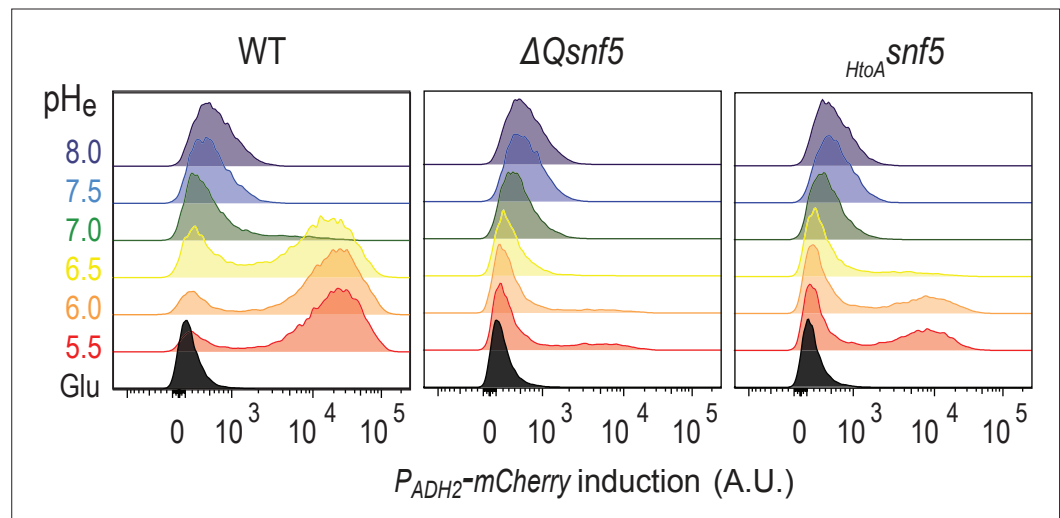


Figure 3—figure supplement 2. P_{ADH2} -mCherry induction requires an acidic extracellular environment and the SNF5 QLC. Cytometry data showing expression levels of the P_{ADH2} -mCherry reporter from WT, $\Delta Qsnf5$, or $HtoA snf5$ cells either growing in glucose (Glu), or 6 hr after acute carbon starvation in media titrated to various pH_e values (these are representative source data for **Figure 3A**).

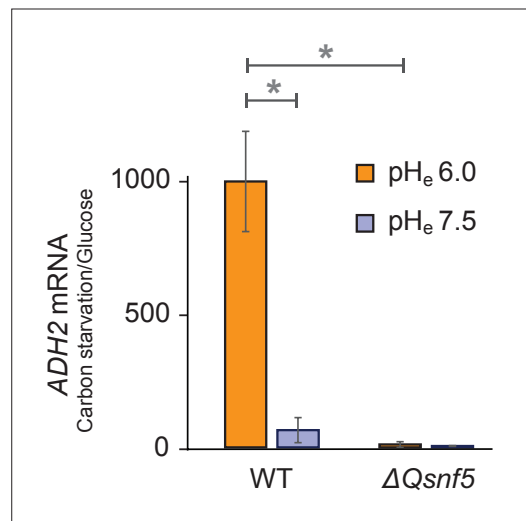


Figure 3—figure supplement 3. Expression of the endogenous *ADH2* mRNA requires an acidic extracellular environment and the *SNF5* QLC. RT-qPCR data showing *ADH2* mRNA levels. The ratio of *ADH2* levels in carbon-starved cells to cells growing in glucose is shown. *ACT1* was used as an internal control to normalize *ADH2* values. WT and $\Delta Qsnf5$ strains were carbon-starved in media titrated to pH_e of either 6.0 or 7.5. Mean and standard deviation of three biological replicates are shown. * and ** represent $p < 0.05$ and $p < 0.01$, respectively, from t-tests.

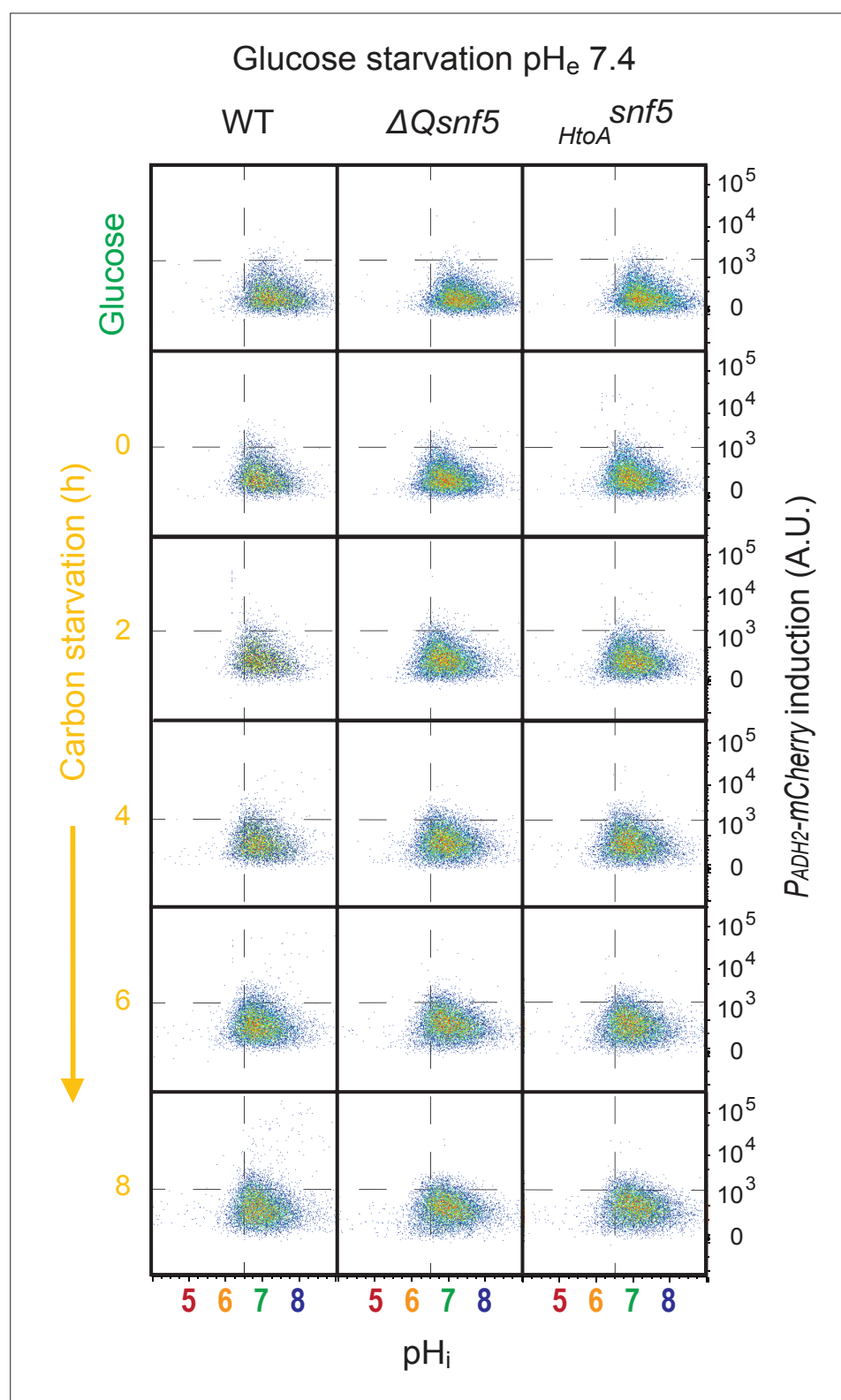


Figure 3—figure supplement 4. Transient acidification of cells requires an acidic extracellular environment. Flow cytometry for WT, $\Delta Qsnf5$, or $HtoA$ *snf5* strains: the x-axis shows nucleocytoplasmic pH (pH_i), while the y-axis shows fluorescence from the P_{ADH2} -mCherry reporter. Panels show cells grown in glucose (top) and then (second to bottom) after 0–8 hr of acute glucose starvation.

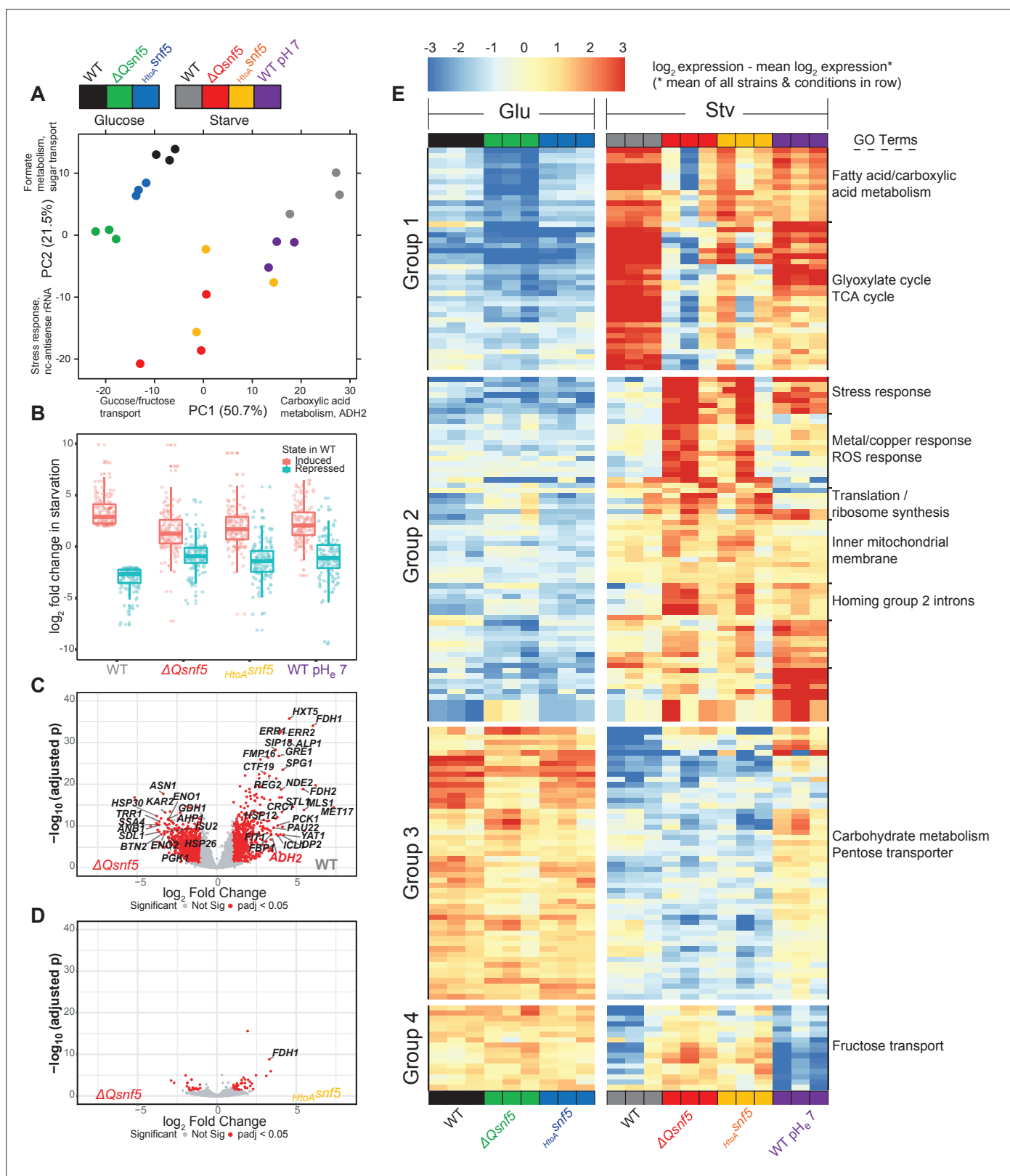


Figure 4. The *SNF5* QLC and acidification of the nucleocytoplasm are required for efficient widespread transcriptional reprogramming upon carbon starvation. (A) Principal component (PC) analysis of three RNA-seq biological replicates for each condition tested. (B) Expression levels of genes that were greater than threefold induced or repressed upon carbon starvation in WT strains are plotted for each *SNF5* allele. (C) Volcano plot showing the \log_2 ratio of expression levels in WT versus $\Delta Qsnf5$ strains (x-axis) and p-values for differential expression (y-axis). Genes with significantly different expression are labeled. (D) Volcano plot showing the \log_2 ratio of expression levels in WT versus $\Delta Qsnf5$ strains (x-axis) and p-values for differential expression (y-axis). Genes with significantly different expression are labeled. Figure 4 continued on next page

Figure 4 continued

expression are indicated in red (\log_2 fold change > 1 and Wald test adjusted p-value < 0.05). (D) Volcano plot as in (C) but comparing expression levels in *HtoA**snf5* strains to $\Delta Qsnf5$ strains. (E) Hierarchically clustered heat map showing expression values of 149 genes with a significant change in expression upon starvation of WT cells (\log_2 fold change > 1 and Wald test adjusted p-value < 0.05). Color code indicates gene expression relative to the mean expression of that gene across all strains and conditions, with red indicating high and blue indicating low values (see legend). Three biological replicates are shown for each experiment. Strain and condition identities are indicated at the bottom of each column. Four groups of genes with similar behavior are indicated to the left. Gene Ontology enrichment results for nine clusters of genes are shown to the right.

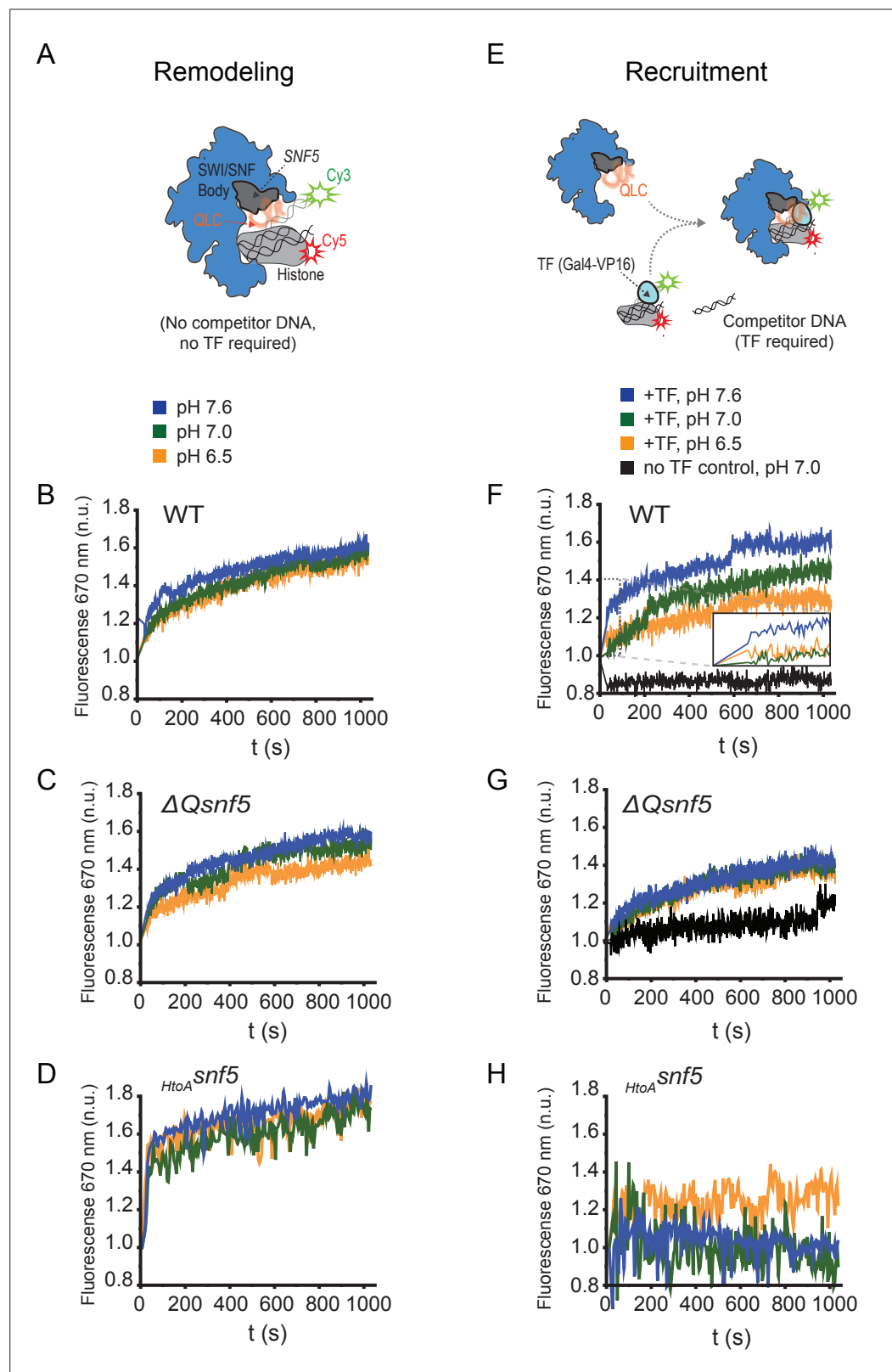


Figure 5. The SNF5 QLC mediates a pH-sensitive transcription factor interaction in vitro. **(A)** Schematic: a Cy3 donor fluorophore was attached to one end of the DNA, and the histone H2A C-termini were labeled with a Cy5 acceptor fluorophore. ATP-dependent mobilization of the nucleosome to the DNA increases Förster resonance energy transfer (FRET), leading to increased emission at 670 nm. **(B)** Representative kinetic traces for

Figure 5 continued on next page

Figure 5 continued

WT (**B**), $\Delta Qsnf5p$ (**C**), and $HtoA^{snf5}$ (**D**) SWI/SNF complexes at pH 7.6 (blue), 7.0 (green), or 6.5 (orange). There is no competitor DNA, so these traces indicate intrinsic remodeling activity without requirement for recruitment by transcription factors. (**E**) Schematic: in the presence of excess competitor DNA, SWI/SNF-dependent remodeling requires recruitment by a transcription factor (Gal4-VP16). (**D**) Representative kinetic traces for WT (**F**), $\Delta Qsnf5p$ (**G**), and $HtoA^{snf5}$ (**H**) SWI/SNF complexes at pH 7.6 (blue), 7.0 (green), or 6.5 (orange). Inset on the WT panel (**F**) shows the first 100 s of the assay after ATP addition. All traces are averages of 2–4 experiments and represent FRET normalized to values prior to addition of ATP.

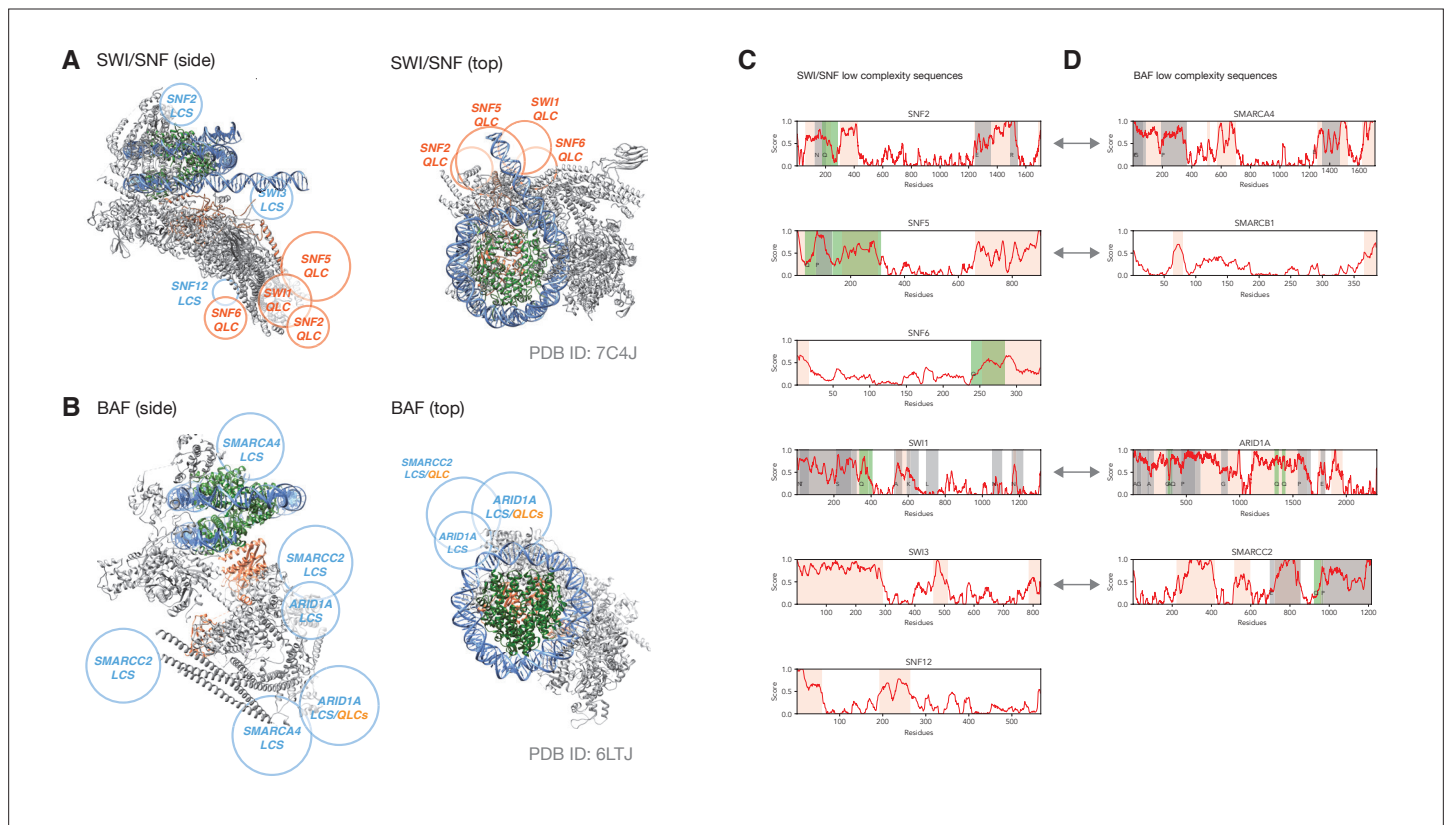


Figure 5—figure supplement 1. QLCs of SWI/SNF cluster around putative transcription factor interaction sites, as do low-complexity sequences of human BAF complex. **(A)** Electron microscopy structure of SWI/SNF (gray) bound to a nucleosome (DNA blue, histones green; PDB ID: 7C4J). The position of SNF5 is highlighted in coral. Rough positions of QLCs are depicted in orange, and large low-complexity sequences are shown in cyan. **(B)** Electron microscopy structure of human BAF complex (gray) bound to a nucleosome (DNA blue, histones green; PDB ID: 6LTJ). The position of ARID1B is highlighted in coral. Rough positions of large low-complexity domains are depicted in cyan, two of which contain short QLCs (indicated in orange). In both cases, top views only highlight sequences that are proximal to the DNA exiting the nucleosome (potential transcription-factor binding site). **(C, D)** Schematics showing predicted low-complexity sequence (orange), including regions enriched for particular amino acids (gray, or green for QLCs). **(C)** shows SWI/SNF subunits and **(D)** shows BAF subunits. Orthology between SWI/SNF and BAF subunits is indicated by gray double-headed arrows.

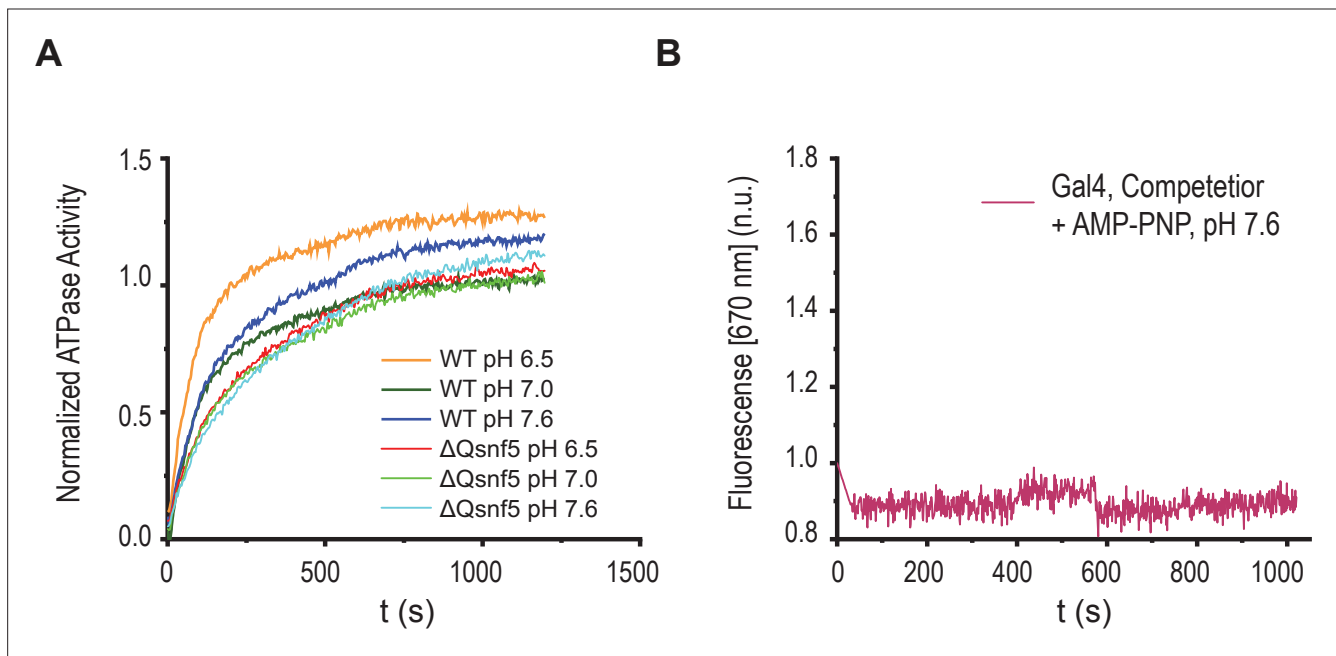


Figure 5—figure supplement 2. Basal ATPase activity is not affected by pH, and Förster resonance energy transfer (FRET) changes require ATP hydrolysis. **(A)** Representative trace of ATPase activity for WT and $\Delta Qsnf5$ mutant SWI/SNF complexes in response to varied environmental pH. WT and mutant complexes do not show significant changes in ATPase activity (as assessed by inorganic phosphate release, see Materials and methods). **(B)** Representative kinetic trace for wild-type SWI/SNF under recruitment conditions after addition of AMP-PNP (a non-hydrolyzable ATP analogue).

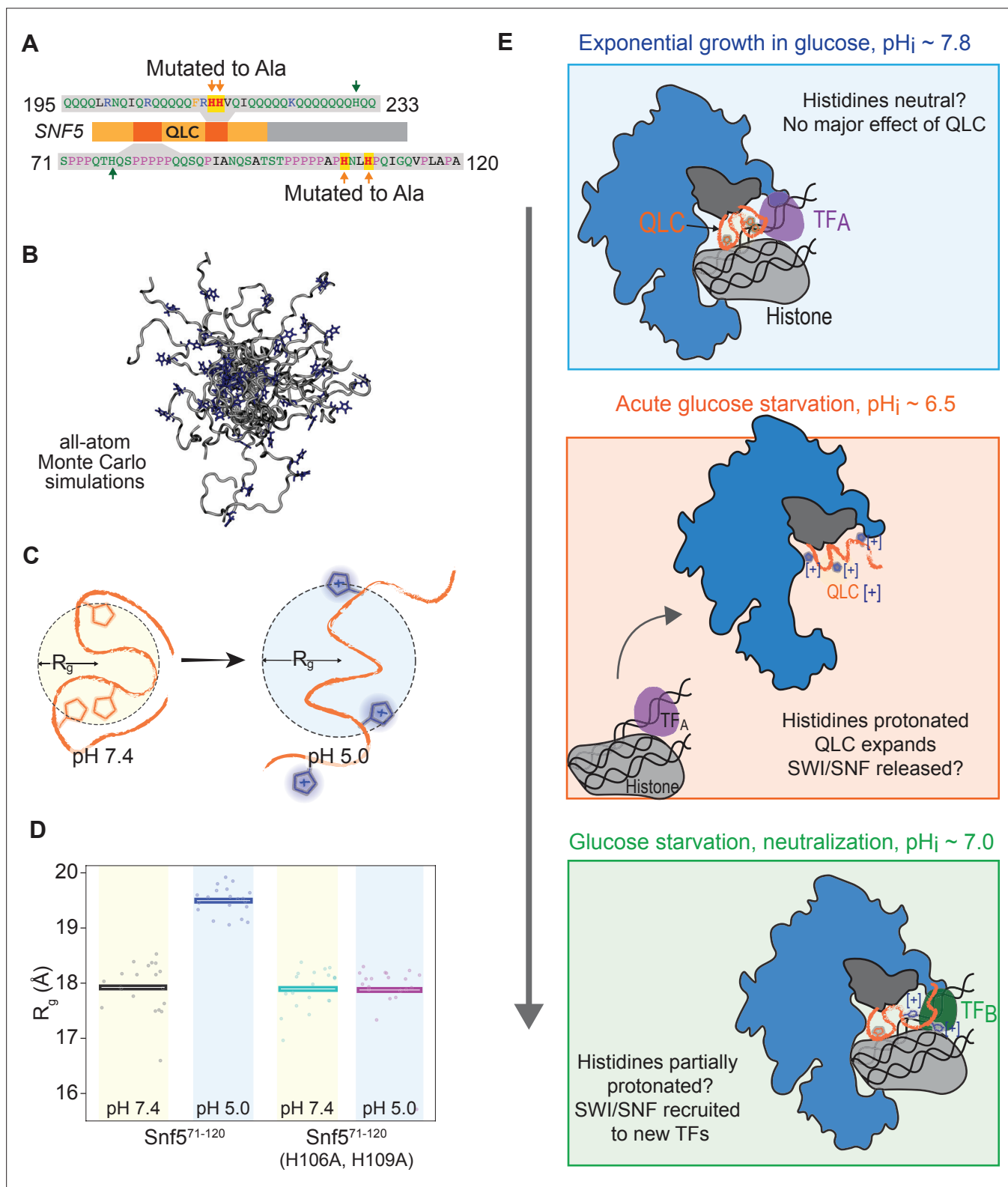


Figure 6. Protonation of histidines leads to conformational expansion of the SNF5 QLC. **(A)** Schematic of the SNF5 gene (center) with the N-terminal QLC in orange and the two simulated peptides in dark orange. Sequences of the simulated peptides and identities of histidines mutated in both the *HtoA*snf5 yeast strain and in simulations are indicated. **(B)** Representative images of conformations sampled in Monte Carlo all-atom simulations. **(C)** Cartoon depicting quantification of radius of gyration (R_g). **(D)** Radius of gyration (R_g , y-axis) of simulations of amino acids 71–120 of the SNF5 QLC with histidines either neutral (pH 7.4) or protonated (pH 5.0). Left two datasets are for the native peptide, right two datasets are with 2/3 histidines (H106 and

Figure 6 continued on next page

Figure 6 continued

H109) replaced with alanine, mimicking the *HtoA**snf5* allele. Points represent the mean R_g from all conformations sampled in each independent simulation (beginning from distinct random initial conformers). Bars represent the mean values of all simulations. **(E)** Model of SWI/SNF regulation during carbon starvation. (Top) In glucose ($\text{pH}_i \sim 7.8$), the *SNF5* QLC is unprotonated. SWI/SNF is engaged by transcription factors that prevent transcription of glucose repressed genes or that activate other genes (TF_A). (Middle) Upon acute carbon starvation, pH_i drops to ~ 6.5 , leading to protonation of histidines in the *SNF5* QLC. Conformational expansion of the QLC may aid the release of SWI/SNF from some transcription factors (TF_A) and potentially drive recruitment to others (not shown). (Bottom) As the cell adapts to carbon starvation, pH_i neutralizes to ~ 7.0 . Histidines within the *SNF5* QLC may be partially protonated? The pK_a of histidine is highly context-dependent. The QLC may aid recruitment of SWI/SNF to the promoters of glucose-repressed genes, thus leading to their expression.

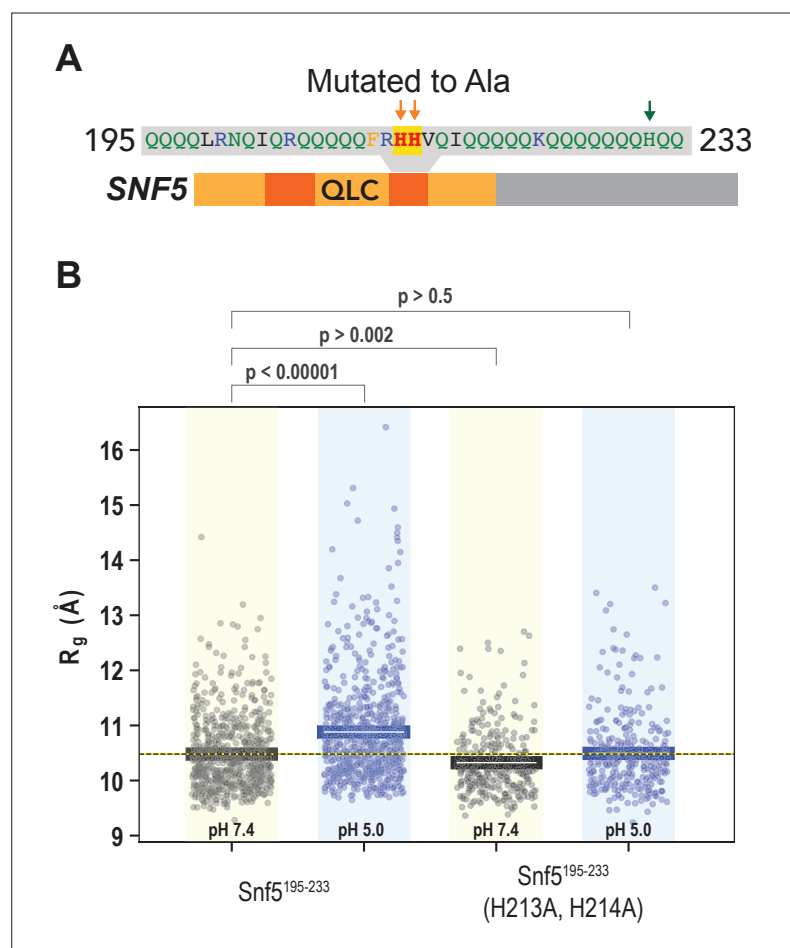


Figure 6—figure supplement 1. A second peptide within the N-terminal QLC of *SNF5* undergoes conformational expansion upon protonation. **(A)** Schematic of the *SNF5* gene, with the sequence and location of the simulated peptide indicated. **(B)** Radius of gyration (R_g , y-axis) of all-atom Monte Carlo simulations of amino acids 195–233 of the *SNF5* QLC with histidines either neutral (pH 7.4) or protonated (pH 5.0). Left two datasets are for the native peptide, right two datasets are with 2/3 histidines (H213 and H214) replaced with alanine, mimicking the *HtoA* *SNF5* allele. Points represent the mean R_g from all conformations sampled in each independent simulation (beginning from distinct random initial conformers). Bars represent the mean values of all simulations. p-Values are from two-sided independent t-tests.